IEEE Photonics Journal
An IEEE Photonics Society Publication

Optical-Stark Induced Distortions in Vortex Momentum Distributions of p-Orbital Electrons of Neon Atoms

Volume 12, Number 6, December 2020

Yufei He
Guizhong Zhang
Jiu Tang
Xin Ding
Jianquan Yao

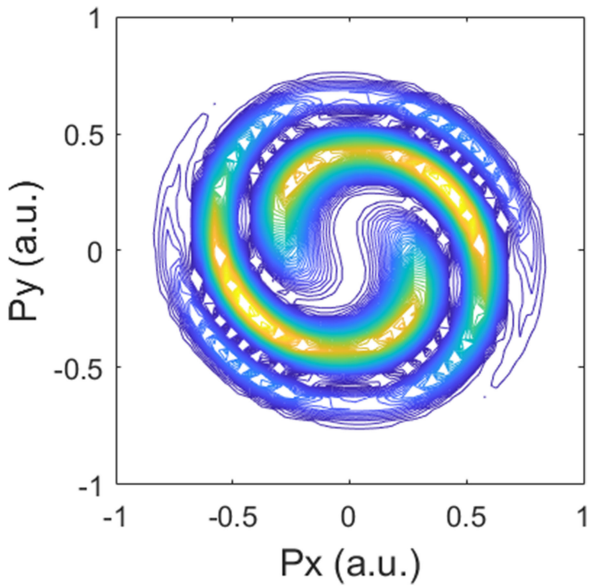

DOI: 10.1109/JPHOT.2020.3037714

Optical-Stark Induced Distortions in Vortex Momentum Distributions of p-Orbital Electrons of Neon Atoms

Yufei He, Guizhong Zhang, Jiu Tang, Xin Ding, and Jianquan Yao

College of Precision Instrument and Optoelectronics Engineering, Key Lab of Optoelectronic Information Technology, Ministry of Education of China, Tianjin University, Tianjin 300072, China

DOI:10.1109/JPHOT.2020.3037714

Manuscript received June 3, 2020; revised October 25, 2020; accepted November 9, 2020. Date of publication November 16, 2020; date of current version December 4, 2020. This work was supported in part by the National Natural Science Foundation of China under Grants 11674243 and 11674242; and in part by State Key Research Program under Grant 2017YFB1401201. Corresponding author: Yufei He (e-mail: johngzhang@tju.edu.cn).

Abstract: We present results of numerical simulations on the photoelectron momentum distributions of the p-orbital electrons of neon atoms ionized by a pair of time-delayed and oppositely circularly polarized intense laser pulses. Deploying the strong-field theory, we can readily produce vortex-shaped momentum distributions. Similarity and disparity in the vortex patterns between the neon and hydrogen atoms are observed. The optical Stark effect is found to induce distortions in the vortex momentum distributions, which are quantitatively described by introducing several physical quantities. Among these quantities, the autocorrelation parameter turns out to be the most sensitive probe for extremely weak Stark effect. The nonlinear phase induced by the optical Stark effect deciphers the distortions of the vortex momentum distributions.

Index Terms: Strong-field photoionization, ultrashort laser pulses, optical Stark effect.

1. Introduction

In the field of atomic, molecular, and optical physics, strong laser pulses are exclusively deployed to induce ionization or dissociation, and either momentum or energy spectra are extensively used to investigate the microscopic processes [1]–[5]. Over the past few years, with the development of femtosecond and attosecond laser technology [6]–[11], circularly polarized laser pulses have been used in some fields especially in the strong field community [12]–[16]. As a result, a Ramsey-type interference of electron wave packets was numerically unveiled to manifest vortex-shaped or spiral-shaped momentum distributions for two time-delayed and oppositely circularly polarized pulses [17]. Experimentally, the vortex momentum distributions were confirmed in potassium atoms [18]. Similar studies were reported: for molecular system, Yuan et al. [19] theoretically studied the photoelectron spectra generated by bi-chromatic circularly polarized attosecond laser pulses in 2016. They found that counter-rotating pulses could produce spiral momentum patterns. For inert atoms, Djiokap [20] numerically investigated the single ionization of helium atom by circularly polarized laser pulses in 2016. They discovered that vortex momentum distributions with zero-start, one-start, three-start, and four-start could appear. Similar work on helium atom were also reported

[21]. Inspired by the pioneering research on the vortex-shaped momentum distributions of atoms and molecules [20], [22]–[29], we undertake numerical simulations on neon atoms exposed to a pair of time-delayed and oppositely circularly polarized intense laser pulses for observing the induced vortex momentum distributions.

Our numerical investigation deploys the strong field approximation (SFA) theory [30]–[32]. Our numerical results show that the vortex-shaped momentum distributions can be readily formed for p-orbital electrons in neon. In addition, we investigate the optical-Stark effect in the neon atoms in order to interrogate its influence on the distortions of the vortex-shaped momentum patterns. To that end, we introduce several physical quantities to quantitatively elucidate the Stark effect and the underlying mechanism. By introducing peak intensity, polar radius, polar angle, angular spans, and autocorrelation parameter for the vortex arms, we have studied the vortex distortions of the photoelectron momentum distributions in depth. Particularly, the autocorrelation parameter turns out to be an extremely sensitive tool to probe the ac-Stark effect. The nonlinear Stark phase induced by this effect successfully deciphers the mechanism of the vortex distortions. As a matter of fact, the optical Stark effect [33]–[35] is an old concept and was once used to prove the correctness of quantum mechanics. The optical-Stark effect, also called dynamic- or ac- Stark effect, is so weak that it is often observed in strong field process. This effect will shift the energy level in accordance with the envelope squared instead of the instantaneous electric field of a laser pulse [36]–[40]. We anticipate that our research outcome could shed light on further investigation on strong field processes of atoms in association with Stark influence.

2. Experimental Details

We deploy the strong field approximation theory (SFA) to perform the numerical simulation. As one of the few analytical theories in the strong field community, SFA has been extensively used in interpreting experimental observations and simulating ionization and dissociation in atomic and molecular systems [41]–[46]. In SFA, the probability amplitude is expressed as:

$$B\ (\boldsymbol{p}) = \mathrm{i}\int_0^{\infty} dt' \boldsymbol{E}\left(t'\right)\boldsymbol{D}\left(\boldsymbol{p}\right)\cdot\exp\left[-iS\left(t'\right)\right] \tag{1}$$

where $\boldsymbol{p}$ is the final momentum of the ionized electrons, $\boldsymbol{D}(\boldsymbol{p})$ is the dipole transition matrix element, and $S(t')$ is the semi-classical action phase which is expressed as:

$$S\ \left(t'\right) = \int_{t'}^{\infty}\left[I_p + (\boldsymbol{p}+\boldsymbol{A})^2/2\right]dt'' + \Delta S\left(t'\right) \tag{2}$$

Unlike hydrogen-like atoms, there is no ansatz for the dipole matrix element to use for neon atom. In Eq. (1), the dipole matrix element, $\boldsymbol{D}(\boldsymbol{p})$ is calculated by using the ground-state wavefunction obtained via the density-functional theory [47], [48] and the final continuum-state wave function taking the form of a plane wave. Therefore, the matrix element is a function of the final momenta of the ionized electron, and can be readily substituted into Eq. (1) for simulating. The second term in Eq. (2) is an extra term introduced to express quantitatively the optical-Stark effect, and will be discussed later.

The laser field used in our numerical simulation is a combination of two counter-rotating circularly polarized pulses with proper temporal delay:

$$\begin{cases} E_x = \frac{\sqrt{2}}{2}\,F\left(t\right)\cdot E_0\cdot\cos\left(\omega t\right) + \frac{\sqrt{2}}{2}F\left(t+\tau\right)\cdot E_0\cdot\cos\left(\omega t+\omega\tau\right) \\ E_y = \frac{\sqrt{2}}{2}\,F\left(t\right)\cdot E_0\cdot\sin\left(\omega t\right) - \frac{\sqrt{2}}{2}F\left(t+\tau\right)\cdot E_0\cdot\sin\left(\omega t+\omega\tau\right) \end{cases}, -\frac{T}{2} < t < \frac{T}{2} \tag{3}$$

where E_0 is the field amplitude of the laser pulses, τ the time delay between the two pulses, T the pulse duration, $F = e^{-\left(\frac{t}{T}\right)^2}$ the pulse envelope function. The plus and minus signs in Eq. (3) can be used to adjust the circular polarizations of the two pulses.

In our simulation, the laser parameters are as follows: frequency ω = 8 - 16 eV, intensity I = 1 $\times$ 10^{14} W/cm^2, pulsewidth T = 1 optical cycle (o.c.), time delay τ = 3 o.c. These parameters were

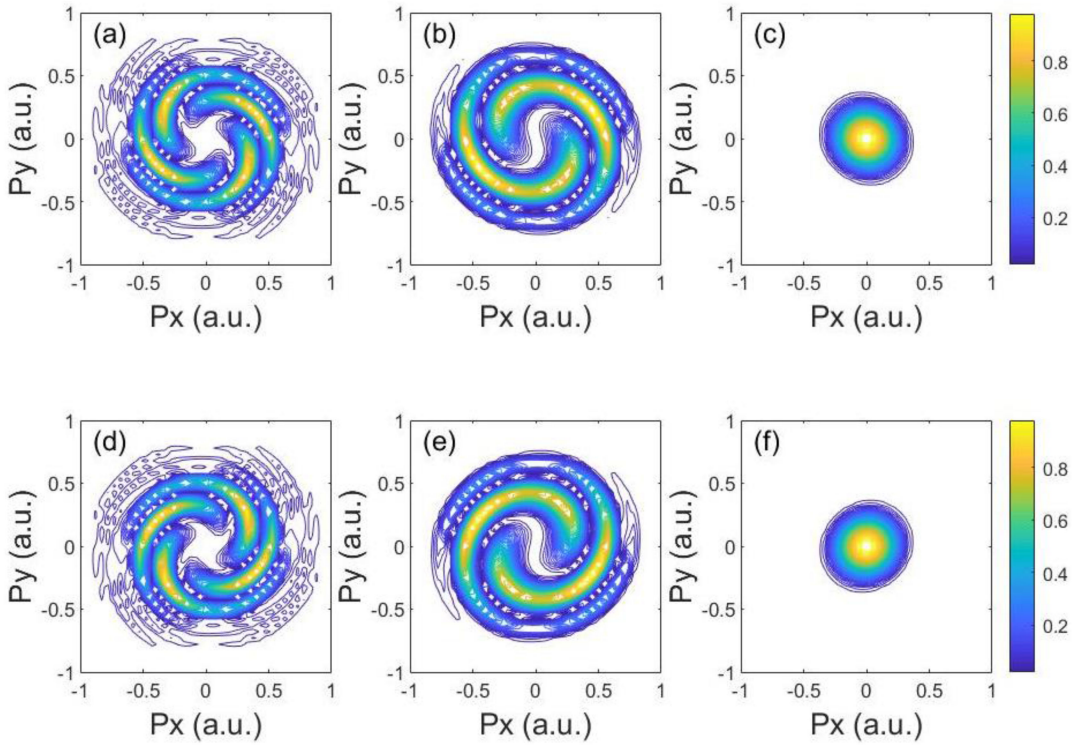

Fig. 1. Photoelectron momentum distributions of p-orbital electrons of neon atoms ionized by a pair of oppositely circularly polarized laser pulses. The simulation parameters are: frequency $\omega = 8$ eV (a, d),12 eV (b, e), 16 eV (c, f), intensity I $= 1 \times 10^{14}$ W/cm^2, pulse width T $= 1$ o.c. and time delay $\tau =$ 3 o.c. Top row is for left/right polarizations (first pulse is left circularly polarized and the second one is right circular polarized), and the bottom row is for right/left polarizations.

made to change over a proper range to confirm that our numerical results are reproducible and robust.

3. Numerical Results and Discussion

We perform extensive numerical simulations on the momentum distributions of p-orbital electrons of the neon atoms exposed to two time-delayed oppositely circularly polarized attosecond pulses. At the beginning, we do not consider the optical-Stark effect and present the obtained momentum distributions in Fig. 1. It is conspicuous that these momentum distributions exhibit symmetric vortex shapes except for a carrier frequency of $\omega = 16$ eV. The Keldysh parameter for our simulation is so small that tunneling ionization is dominant. In our simulation, the carrier frequency ω is chosen to be 8 eV, 12 eV and 16 eV, and too short or too long delays will not induce vortex patterns. In order to discuss the properties of the vortex momentum distributions of the ionized p-orbital electrons, we also conduct similar simulation for the s-orbital electrons in neon. For theses s-orbital electrons, our results show that the number of the vortex arms in the momentum distributions is equal to the total number of photons required to over the ionization threshold. For the p-orbital electrons, however, this rule no longer holds. Our calculation of the ionization potential for the p-orbital electrons by the density functional theory gives an ionization potential of 21.5 eV. For example, for $\omega = 12$ eV, two photons were required to overcome the 21.5 eV ionization potential if this rule held, then a four-fold symmetric vortex pattern would appear. The fact is that the momentum patterns in Fig. 1(b) and (e) all show two-fold symmetry. When the photon energy is further increased to $\omega = 16$ eV, featureless patterns appear in the photoelectron momentum distributions. These distinctive vortex behaviors

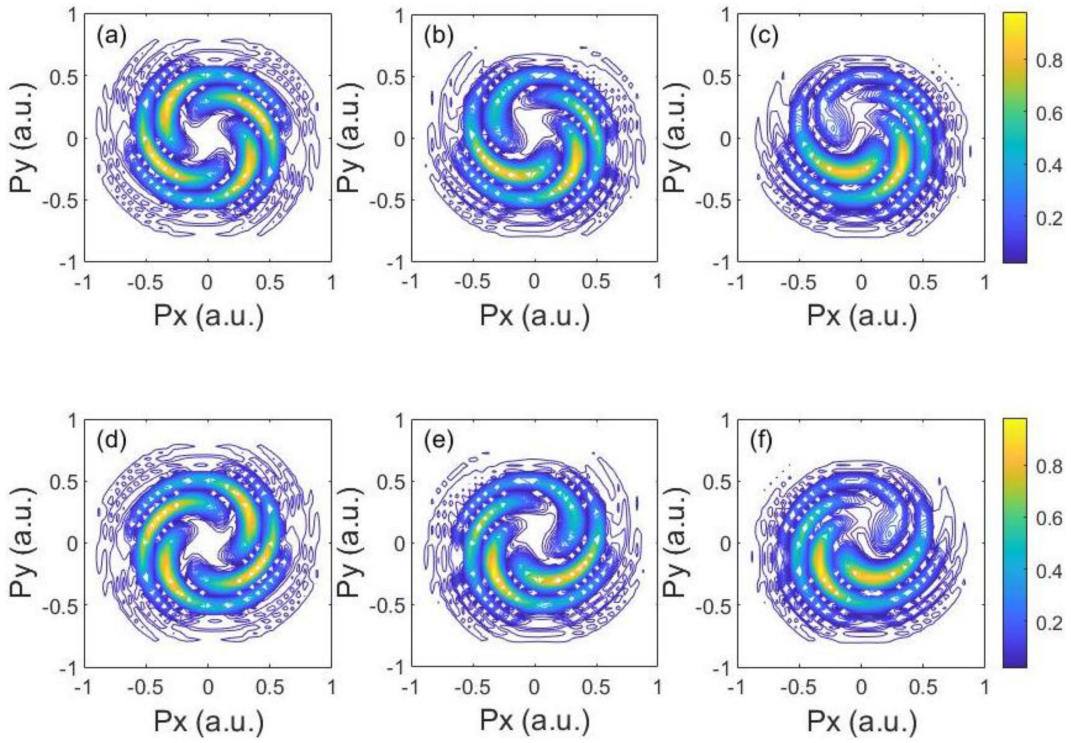

Fig. 2. Distorted vortex shapes of the momentum distributions of p-orbital electrons considering the optical-Stark effect. The Stark coefficient is $\alpha = 0$ (a, d), 0.005 (b, e), 0.01 (c, f). The carrier frequency is $\omega = 8$ eV and other parameters are the same as in Fig. 1.

are attributed to the properties of the dipole matrix element of the p-orbital electrons which is quite different from that of hydrogen. Another observation with the vortex patterns in Fig. 1 is that the vortex helicity is the same as for the s-orbital electrons and for the hydrogen atoms [27]. In other words, the spiral arms are right-polarized if the first pulse is left circularly polarized and the second one is right circularly polarized. We also confirm that the momentum distributions will show no vortex shape if the two laser pulses have identical circular polarizations. We anticipate that p-orbital electrons of other inert atoms will show similar vortex patterns.

We now consider the optical Stark effect on the p-orbital electrons. The down-shift of the ground state energy level can be considered equivalent to an up-shift of the ionization potential. And the dipole matrix element will also be altered. As appeared in Eq. (2), the ionization potential, I_p, will be added by an extra term of $\alpha[F^2(t) + F^2(t+\tau)]$ to count this effect, and a coefficient α is introduced here to quantitatively describe the strength of the effect. The momentum distributions are re-simulated taking into account of the optical-Stark effect. The resultant vortex shapes of the momentum distributions are found distorted, as shown in Fig. 2 for a few typical patterns. We focus on situation with a carrier frequency of $\omega = 8$ eV and a range of Stark coefficient α. It is clear from Fig. 2 that the distortions of the vortex momentum distributions becomes more and more significant as the Stark coefficient α is increased. Our numerical simulation reveals that the vortex distortions is independent of the helicity of the spiral rotation [27], as shown in the top and bottom panels in Fig. 2. The results prove that the photoelectron momentum distributions for the p-orbital electrons in neon atoms have a sensitive response to the optical-Stark effect. In addition, our simulation shows that this effect has little influence on the vortex-free momentum distributions like those in Fig. 1(c) and (f).

In order to quantitatively analyze the vortex distortions induced by the optical-Stark effect, we propose several quantities to evaluate the extent to which the distortions of the photoelectron

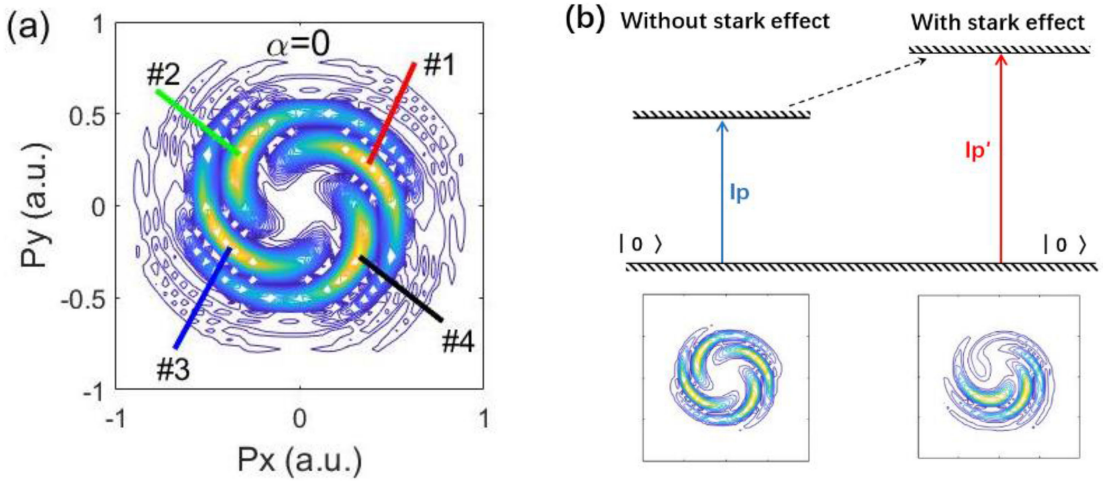

Fig. 3. (a) Numbering of the vortex arms in the momentum distributions for quantitative analysis of the distortions of the vortex shapes of the photoelectron momentum distributions induced by optical-Stark effect; (b) Illustrative sketch of the optical-Stark effect on the ionization potential I_p.

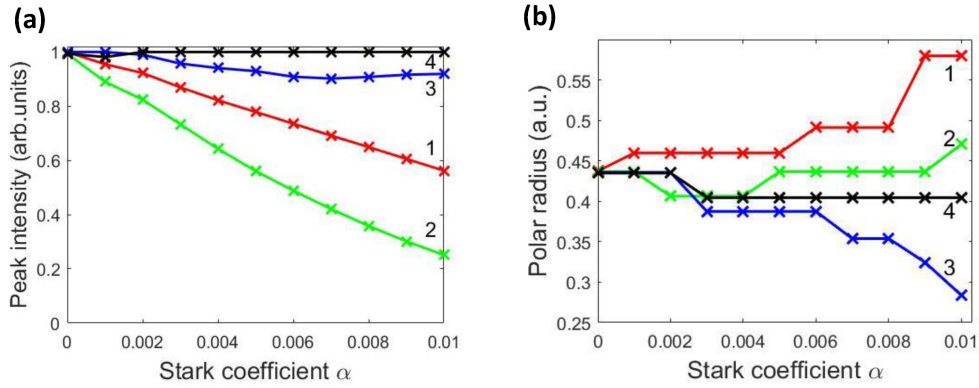

Fig. 4. (a) Variations of the peak intensities of the four vortex arms with the Stark coefficient. It is clear that vortex arms #1 and #2 experience maximal changes; (b) Variations of the polar radii of the four vortex arms with the Stark coefficient. It is clear that vortex arms #1 and #3 experience maximal changes. The numbers and colors of the curves correspond to those given in Fig. 3.

momentum distributions vary with the Stark coefficient α. We start by defining, in Fig. 3, the numbering of the vortex arms: the first vortex arm is the one mostly located in the first quadrant, the second vortex arm is the one mostly located in the second quadrant, and so on. We then investigate the peak intensity, polar radius of the peak, polar angle and angular range and auto-correlation of these vortex arms, and how they react to the optical-Stark effect.

Peak intensities and the polar radii of the four vortex arms are obtained directly from the momentum distributions. The dependence of these quantities upon the Stark coefficient α is given as curves in Fig. 4(a) and (b), respectively. It is seen from Fig. 4(a) that with the increase of the Stark coefficient α, the intensity values at the peaks of the vortex arms #1 and #2 decrease dramatically, while those of the vortex arms #3 and #4 show little variations. In addition, our vast simulations show that these trends still hold true when the Stark coefficient α is further increased until the vortex arms #1 and #2 almost fade out while the vortex arms #3 and #4 remain observable. Pertaining to the polar radii in Fig. 4(b), they also demonstrate some law: with the increase of the Stark coefficient

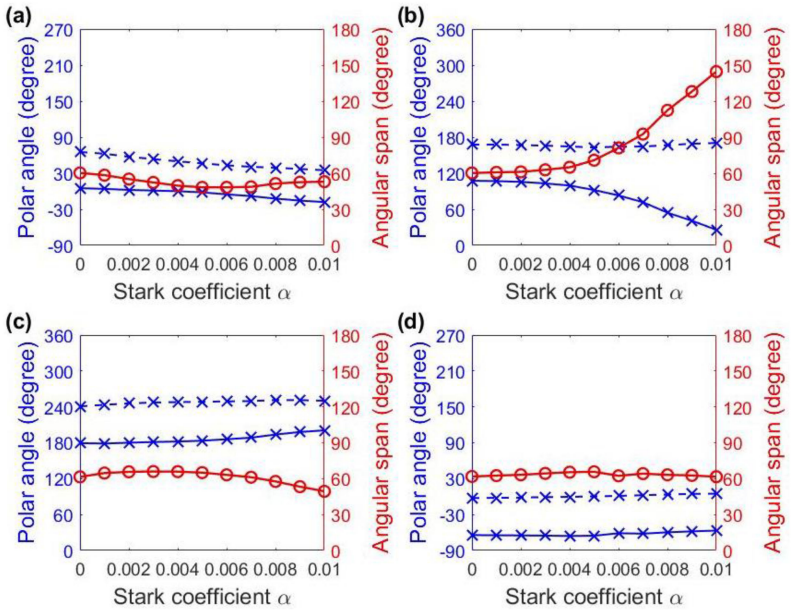

Fig. 5. Dependence of the polar angles and the angular spans of the four vortex arms on the Stark coefficient. Blue color denotes the starting and ending polar angles and the red color denotes the angular spans, respectively.

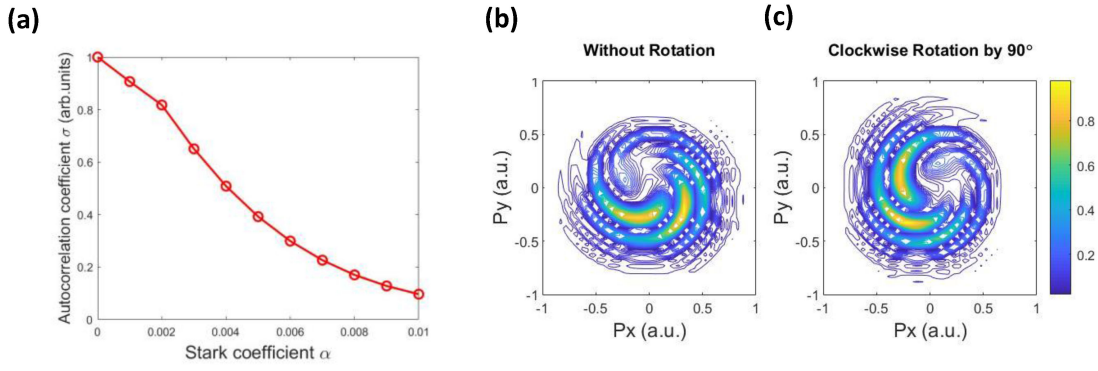

Fig. 6. (a) Autocorrelation curve of the vortex patterns. It is seen that the variation of the autocorrelation parameter with the optical-Stark coefficient is monotonic and almost linear; (b) Distorted vortex patterns set for $\alpha = 0.01$; (c) Clockwise rotation of the distorted vortex patterns set in (b) by 90 degrees. A successive rotation by 90 degrees produces the four sets for calculating the autocorrelation curve.

α, vortex arm #1 gradually moves outward from the origin, while vortex arms #3 moves closer to the origin. In contrast, the vortex arms #2 and #4 do not show drastic changes.

As to the polar angles, we utilize a contour-like scheme to interrogate the impact of the optical-Stark effect on the vortex patterns distortions. Namely, for each vortex arm, we define a starting and an ending polar angle at which the intensity values of a vortex arm descend to $1/\sqrt{2}$ of its peak intensity value. We plot, in Fig. 5, the Stark coefficient dependence of the starting and ending angles and the corresponding angular spans (difference between the starting and ending angles) of all the four vortex arms. The first observation from these figures is that both the starting and ending angles do not manifest prominent changes with the Stark strength. The angular spans, however, show quite different behaviors. It is clear that the angular span for vortex arm #2 is increasing from 60 to 150 degrees, and those of vortex arms #1, #3 and #4 remain roughly unchanged at 60 degrees. As the angular span measures the extension of a vortex arm, the behavior of vortex

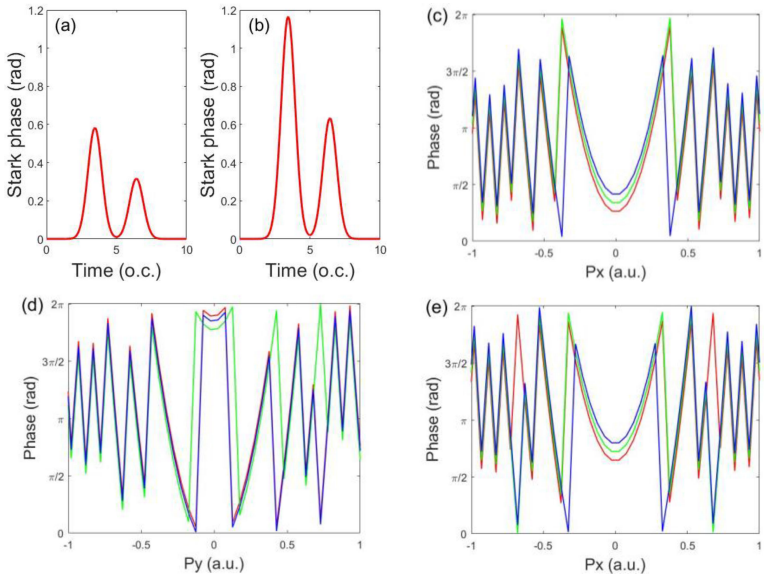

Fig. 7. (a) and (b) Variations of the Stark phase versus time for Stark coefficient $\alpha = 0.005$ and 0.01; (c) Variations of the total phase (classical action phase and the Stark phase) versus momentum Px at Py $= 0$ and at a time instant of 7 o.c.; (d) Total phase versus Py at Px $= 0.4$ a.u. and at a time instant of 7 o.c. (e) Total phase versus Px at Py $= 0.25$ a.u. and at a time instant of 7 o.c. The color legends are: red, green, and blue correspond to three different Stark coefficients of $\alpha = 0$, 0.005 and 0.01.

arm #2 means that this vortex arm is stretched longer compared to others due to the onset of the optical-Stark effect. Other choice of the starting and ending polar angles will not affect the analysis. The uneven vortex distortion is caused by the uneven impact of the nonlinear phase, as discussed later. All our above observations show that different quantities such as vortex peak intensity, vortex polar radius and vortex angular span respond to the optical-Stark effect in quite different ways both qualitatively and quantitatively. We believe that the dipole matrix element of the p-orbital electrons renders the performance of these vortex arms.

In order to further explore the optical-Stark effect in the distortions of the vortex photoelectron momentum distributions, we introduce another quantity ρ to evaluate the degrees of the distortions. The concept of ρ implies autocorrelation, therefore, ρ is referred to as the autocorrelation parameter. By labeling the momentum distributions as a set {p} and a new momentum distributions after a clockwise rotation of {p} by θ degrees as another set {p(θ)}, with p denoting the elements of the photoelectron momentum distributions, we can calculate the autocorrelation parameter as $\rho = \sum p * p(90) * p(180) * p(270)$. It is the sum of the product of four sets of elements p, p(90), p(180), and p(270) in corresponding positions. Fig. 6 gives the computed autocorrelation parameter ρ as a function of the Stark coefficient α, and an illustration of the formation of the four momentum sets. It is observed that ρ decreases almost linearly with α, which convinces us that the autocorrelation parameter is an excellent indicator of the optical-Stark effect in the photoelectron momentum distributions. When the Stark coefficient α is equal to 0.005, for example, the influence of optical-Stark effect on the vortex patterns is insignificantly sensible (Fig. 2(b, e)). However, as demonstrated in Fig. 6, the autocorrelation parameter drastically drops from 1 to 0.39 when the Stark coefficient is changed from $\alpha = 0$ to a small value of $\alpha = 0.005$.

For deciphering the mechanism behind the distortions of the vortex patterns induced by the optical-Stark effect, we calculate the additional Stark phase which is defined as:

$$\Delta S\ (t') = \int_{t'}^{\infty} dt'' \left\{ I_p \alpha \left[F^2 (t'') + F^2 (t'' + \tau) \right] \right\} \tag{4}$$

Our analysis shows that the Stark phase plays a uniquely important role in the distortions. According to Eq. (4), the additional Stark phase is a function of time, and the total phase of Eq. (2)

including the classical action and the Stark effect is a function of both time and momentum, as shown in Fig. 7. From Fig. 7(a) and (b), one can confirm that the relationship between the additional Stark phase and the Stark coefficient is linear, because the ratio between the ordinate values of the two peaks at about 3.5 o.c. in Figs. 7(a) and (b), exactly equal to the ratio of the corresponding Stark coefficients of 0.005 to 0.01. One also sees that the maximal values of the additional Stark phase appear at the crests of the two pulse envelopes and that the optical-Stark effect is most active in the time period of 2 o.c. to 8 o.c. Therefore, we choose to show the total phase versus momentum at a time instant of 7 o.c. for different Stark coefficients in Fig. 7(c), (d), and (e).

It is observed from Fig. 7(c) that the total phase experiences the markedly alterations at approximately Px $= -0.4$ and 0.4 a.u. when the Stark coefficient α is increased from 0 to 0.01. From Fig. 7(d) it is seen that the phase alterations suffer a asymmetric variation for the negative and positive Py values and the alterations are most prominent at about Py $= 0.4$ a.u. which coincides with the most distorted vortex arms #1. A comparison between the curves in Fig. 7(c) and (e) shows that the phase alterations mostly occur at around Px $= -0.4$ and 0.4 a.u. at which the most distorted vortex arms #1 and #2 locate. To further prove the function of the time-dependent nonlinear phase, we try a constant phase and linearly time dependent phase in Eq. (4) to re-simulate the vortex momentum patterns and find no distortions. All these results prove that it is the nonlinear time-dependent phase induced by the optical Stark effect that causes the distortions of the vortex momentum distributions.

4. Conclusion

By deploying the SFA theory, we have performed extensive numerical simulations on the vortex momentum distributions of p-orbital electrons of neon atoms ionized by a pair of time-delayed and oppositely circularly polarized intense laser pulses. Vortex-shaped momentum distributions are readily generated and disparity from the hydrogenlike system is observed. We introduce several physical quantities to quantitatively elucidate the optical Stark effect and the autocorrelation parameter turns out to be the most sensitive probe for extremely weak Stark effect. The nonlinear phase induced by this effect deciphers the distortions of the vortex momentum distributions. The vortex momentum patterns are anticipated to be a sensitive tool for interrogating the optical Stark effect in strong field processes.

References

[1] T. Brabec, *Strong Field Laser Physics*. New York, NY, USA: Springer, 2008.
[2] A. N. Grum-Grzhimailo, A. D. Kondorskiy, and K. Bartschat, "Controlling the angular distribution of atomic photoelectrons in the region of laser-induced continuum structure in the femtosecond time domain," *J. Phys. B, At. Mol. Opt. Phys.*, vol. 39, no. 22, pp. 4659–4671, 2006.
[3] L. Peng and A. F. Starace, "Attosecond pulse carrier-envelope phase effects on ionized electron momentum and energy distributions," *Phys. Rev. A.*, vol. 76, no. 4, 2007, Art. no. 043401.
[4] M. Li *et al.*, "Spatial-temporal control of interferences of multiple tunneling photoelectron wave packets," *Phys. Rev. A.*, vol. 92, no. 1, 2015, Art. no. 013416.
[5] N. Douguet, A. N. Grum-Grzhimailo, E. V. Gryzlova, E. I. Staroselskaya, J. Venzke, and K. Bartschat, "Photoelectron angular distributions in bichromatic atomic ioniza polarized VUV femtosecond pulses," *Phys. Rev. A.*, vol. 93, no. 3, 2016, Art. no. 033402.
[6] D. E. Spence, P. N. Kean, and W. Sibbett, "60-fsec pulse generation from a self-mode-locked Ti:Sapphire laser," *Opt. Lett.*, vol. 16, no. 1, pp. 42–44, 1991.
[7] C. Spielmann, F. Krausz, T. Brabec, E. Wintner, and A. J. Schmidt, "Femtosecond passive mode locking of a solid-state laser by a dispersively balanced nonlinear interferometer," *Appl. Phys. Lett.*, vol. 58, no. 22, pp. 2470–2472, 1991.
[8] P. M. Paul *et al.*, "Observation of a train of attosecond pulses from high harmonic generation," *Science*, vol. 292, no. 5522, pp. 1689–1692, 2001.
[9] U. Keller, "Femtosecond to attosecond optics," *IEEE Photon. J*, vol. 2, no. 2, Apr. 2010.
[10] K. J. Yuan and A. D. Bandrauk, "Single circularly polarized attosecond pulse generation by intense few cycle elliptically polarized laser pulses and terahertz fields from molecular media," *Phys Rev Lett*, vol. 110, no. 2, 2013, Art. no. 023003.
[11] E. Cunningham and Z. Chang, "Optical gating with asymmetric field ratios for isolated attosecond pulse generation," *IEEE J. Sel. Topics Quantum Electron*, vol. 21, no. 5, pp. 1–6, Sept./Oct. 2015.
[12] M. Abu-Samha and L. B. Madsen, "Interrogation of orbital structure by elliptically polarized intense femtosecond laser pulses," *Phys. Rev. A.*, vol. 84, no. 2, 2011, Art. no. 023411.

[13] Y. Zhou, C. Huang, A. Tong, Q. Liao, and P. Lu, "Correlated electron dynamics in nonsequential double ionization by orthogonal two-color laser pulses," *Opt. Exp.*, vol. 19, no. 3, pp. 2301–2308, Jan. 2011.
[14] J. Geng, W. Xiong, X. Xiao, L. Peng, and Q. Gong, "Nonadiabatic electron dynamics in orthogonal two-color laser fields with comparable intensities," *Phys. Rev. Lett.*, vol. 115, no. 19, 2015, Art. no. 193001.
[15] M. Li *et al.*, "Spatial-temporal control of interferences of multiple tunneling photoelectron wave packets," *Phys. Rev. A.*, vol. 92, 2015, Art. no. 013416.
[16] S. Wang *et al.*, "Angular momentum-dependent transmission of circularly polarized vortex beams through a plasmonic coaxial nanoring," *IEEE Photon. J.*, vol. 10, no. 1, pp. 1–9, 2018, Art. no. 5700109.
[17] J. M. Ngoko Djiokap, S. Hu, L. B. Madsen, N. L. Manakov, A. V. Meremianin, and A. F. Starace, "Electron vortices in photoionization by circularly polarized attosecond pulses," *Phys. Rev. Lett.*, vol. 115, no. 11, 2015, Art. no. 113004.
[18] D. Pengel, S. Kerbstadt, D. Johannmeyer, L. Englert, T. Bayer, and M. Wollenhaupt, "Electron vortices in femtosecond multiphoton ionization," *Phys. Rev. Lett.*, vol. 118, 2017, Art. no. 053003.
[19] K. Yuan, S. Chelkowski, and A. D. Bandrauk, "Photoelectron momentum distributions of molecules in bichromatic circularly polarized attosecond UV laser fields," *Phys. Rev. A.*, vol. 93, no. 5, 2016, Art. no. 053425.
[20] J. M. Ngoko Djiokap, A. V. Meremianin, N. L. Manakov, S. Hu, L. B. Madsen, and A. F. Starace, "Multistart spiral electron vortices in ionization by circularly polarized UV pulses," *Phys. Rev. A*, vol. 94, no. 1, 2016, Art. no. 013408.
[21] J. M. Ngoko Djiokap, A. V. Meremianin, N. L. Manakov, S. Hu, L. B. Madsen, and A. F. Starace, "Kinematical vortices in double photoionization of helium by attosecond pulses," *Phys. Rev. A.*, vol. 96, 2017, Art. no. 013405.
[22] M. Harris, C. A. Hill, and J. M. Vaughan, "Optical helices and spiral interference fringes," *Opt. Commun.*, vol. 106, no. 4 – 6, pp. 161–166, Mar. 1994.
[23] E. Hasovic, W. Becker, and D. B. Milosevi, "Electron rescattering in a bicircular laser field," *Opt. Exp.*, vol. 24, no. 6, pp. 6413–6424, 2016.
[24] J. M. Ngoko Djiokap, S. Hu, L. B. Madsen, N. L. Manakov, A. V. Meremianin, and A. F. Starace, "Electron vortices in photoionization by circularly polarized attosecond pulses," *Phys. Rev. Lett.*, vol. 115, Sep. 2015, Art. no. 113004.
[25] K. Yuan, S. Chelkowski, and A. D. Bandrauk, "Photoelectron momentum distributions of molecules in bichromatic circularly polarized attosecond UV laser fields," *Phys. Rev. A.*, vol. 93, no. 5, 2016, Art. no. 053425.
[26] D. Pengel, S. Kerbstadt, D. Johannmeyer, L. Englert, T. Bayer, and M. Wollenhaupt, "Electron vortices in femtosecond multiphoton ionization," *Phys. Rev. Lett.*, vol. 118, 2017, Art. no. 053003.
[27] M. Li, G. Zhang, X. Kong, T. Wang, X. Ding, and J. Yao, "Dynamic stark induced vortex momentum of hydrogen in circular fields," *Opt. Exp.*, vol. 26, no. 2, pp. 878–886, Jan. 2018.
[28] M. Li, G. Zhang, X. Ding, and J. Yao, "Symmetric electron vortices of hydrogen ionized by orthogonal elliptical fields," *IEEE Photon. J*, vol. 10, no. 4, Aug. 2018, Art. no. 3300109.
[29] M. Li, G. Zhang, X. Ding, and J. Yao, "AC stark effect on vortex spectra generated by circularly polarized pulses," *IEEE Photon. J*, vol. 11, no. 3, Jun. 2019, Art. no. 3300111.
[30] L. V. Keldysh, "Ionization in the field of a strong electromagnetic wave," *Sov. Phys. - JETP*, vol. 20, pp. 1307–1314, Jan. 1965.
[31] F. H. M. Faisal, "Multiple absorption of laser photons by atoms," *J. Phys. B*, vol. 6, no. 4, pp. L89–L92, May 1973.
[32] H. R. Reiss, "Effect of an intense electromagnetic field on a weakly bound system," *Phys. Rev. A.*, vol. 22, no. 5, pp. 1786–1813, Nov. 1980.
[33] S. H. Autler and C. H. Townes, "Stark effect in rapidly varying fields," *Phys. Rev.*, vol. 100, no. 2, pp. 703–722, Oct. 1955.
[34] H. C. Ohanian, *Principles of Quantum Mechanics*. Engle wood Cliffs, NJ, USA: Prentice-Hall, 1990.
[35] E. Merzbacher, *Quantum Mechanics*, 3rd ed. New York, NY, USA: Wiley, 1998.
[36] N. B. Delone and V. P. Krainov, "AC stark shift of atomic energy levels," *Phys. Uspekhi*, vol. 42, no. 7, pp. 669–687, Oct. 2007.
[37] R. Loudon, *The Quantum Theory of Light*. London. U.K: Oxford Univ. Press, 2000.
[38] C. Gerry and P. Knight, *Introductory Quantum Optics*. Cambridge, U.K.: Cambridge Univ. Press, 2004.
[39] W. L. Zhang, X. M. Wu, F. Wang, R. Ma, X. F. Li, and Y. J. Rao, "Stark effect induced microcavity polariton solitons," *Opt. Exp.*, vol. 23, no. 12, pp. 15762–15767, Jun. 2015.
[40] C. Yu and L. B. Madsen, "Sequential and nonsequential double ionization of helium by intense XUV laser pulses: Revealing ac stark shifts from joint energy spectra," *Phys. Rev. A*, vol. 94, no. 5, 2016, Art. no. 053424.
[41] M. Lewenstein, P. Salières, and A. L'Huillier, "Phase of the atomic polarization in high-order harmonic generation," *Phys. Rev. A.*, vol. 52, pp. 4747–4754, Jan. 1995.
[42] E. Hasović, M. Busuladžić, A. Gazibegović-Busuladžić, D. B. Milosevic, and W. Becker, "Simulation of above-threshold ionization experiments using the strong-field approximation," *Laser Phys*, vol. 17, no. 4, pp. 376–389, Apr. 2007.
[43] E. Hasović, M. Busuladžić, W. Becker, and D. B. Milosevic, "Dressed-bound-state molecular strong-field approximation: Application to above-threshold ionization of heteronuclear diatomic molecules," *Phys. Rev. A.*, vol. 84, 2011, Art. no. 063418.
[44] C. Yu and L. B. Madsen, "Above-threshold ionization of helium in the long-wavelength regime: Examining the single-active-electron approximation and the two-electron strong-field approximation," *Phys. Rev. A.*, vol. 95, no. 6, 2017, Art. no. 063407.
[45] M. Klaiber, J. Danek, E. Yakaboylu, K. Z. Hatsagortsyan, and C. H. Keitel, "Strong-field ionization via a high-order Coulomb-corrected strong-field approximation," *Phys. Rev. A.*, vol. 95, 2017, Art. no. 023403.
[46] C. Yu and L. B. Madsen, "Above-threshold ionization of helium in the long-wavelength regime: Examining the singleactive-electron approximation and the two-electron strong-field approximation," *Phys. Rev. A.*, vol. 95, 2017, Art. no. 063407.
[47] H. A. Bethe and E. E. Salpeter, *Quantum Mechanics of One and Two Electron Atoms*, Berlin, Germany: Springer-Verlag, 1957.
[48] M. Lewenstein, P. Balcou, M. Y. Ivanov, A. L'Huillier, and P. B. Corkum, "Theory of high-harmonic generation by low-frequency laser fields," *Phys. Rev. A.*, vol. 49, no. 3, pp. 2117–2132, Apr. 1994.